Electronic Correlation and Pseudogap-Like Behavior of High-Temperature Superconductor $La_3Ni_2O_7$

Yidian Li(李义典)[1†], Xian Du(杜宪)[1†], Yantao Cao(曹延涛)[2,3†], Cuiying Pei(裴翠颖)[4†], Mingxin Zhang(张明鑫)[4], Wenxuan Zhao(赵文轩)[1], Kaiyi Zhai(翟恺熠)[1], Runzhe Xu(许润哲)[1], Zhongkai Liu(柳仲楷)[4,5], Zhiwei Li(李志伟)[2], Jinkui Zhao(赵金奎)[3], Gang Li(李刚)[4], Yanpeng Qi(齐彦鹏)[4,5,6*], Hanjie Guo(郭汉杰)[3*], Yulin Chen(陈宇林)[4,5,7*], and Lexian Yang(杨乐仙)[1,8*]

[1]*State Key Laboratory of Low Dimensional Quantum Physics, Department of Physics, Tsinghua University, Beijing 100084, China*
[2]*Key Lab for Magnetism and Magnetic Materials of the Ministry of Education, Lanzhou University, Lanzhou 730000, China*
[3]*Songshan Lake Materials Laboratory, Dongguan 523808, China*
[4]*School of Physical Science and Technology, ShanghaiTech University, Shanghai 201210, China*
[5]*ShanghaiTech Laboratory for Topological Physics, Shanghai 200031, China*
[6]*Shanghai Key Laboratory of High-Resolution Electron Microscopy, ShanghaiTech University, Shanghai 201210, China*
[7]*Department of Physics, Clarendon Laboratory, University of Oxford, Parks Road, Oxford OX1 3PU, UK*
[8]*Frontier Science Center for Quantum Information, Beijing 100084, China*

(Received 1 July 2024; accepted manuscript online 12 July 2024)

High-temperature superconductivity (HTSC) remains one of the most challenging and fascinating mysteries in condensed matter physics. Recently, superconductivity with transition temperature exceeding liquid-nitrogen temperature is discovered in $La_3Ni_2O_7$ at high pressure, which provides a new platform to explore the unconventional HTSC. In this work, using high-resolution angle-resolved photoemission spectroscopy and *ab initio* calculation, we systematically investigate the electronic structures of $La_3Ni_2O_7$ at ambient pressure. Our experiments are in nice agreement with *ab initio* calculations after considering an orbital-dependent band renormalization effect. The strong electron correlation effect pushes a flat band of d_{z^2} orbital component below the Fermi level (E_F), which is predicted to locate right at E_F under high pressure. Moreover, the $d_{x^2-y^2}$ band shows pseudogap-like behavior with suppressed spectral weight and diminished quasiparticle peak near E_F. Our findings provide important insights into the electronic structure of $La_3Ni_2O_7$, which will shed light on understanding of the unconventional superconductivity in nickelates.

DOI: 10.1088/0256-307X/41/8/087402

Being a long-standing problem yet to be resolved, high-temperature superconductivity (HTSC) exhibits important scientific significance and application prospects.[1–3] Up to date, there are only two families of compounds featuring unconventional superconductivity well above the McMillan limit at ambient pressure: cuprates and iron-based superconductors (Fe-SCs).[1–3] Both of them show layered crystal structures; the electronic states near the Fermi level (E_F) are dominated by $3d$ electrons with strong electronic correlation;[1–4] and the superconductivity is in proximity to a magnetic phase in their phase diagrams.[5,6] However, prominent differences also exist between these two families of superconductors. Cuprates based on $3d^9$ electronic configuration of Cu^{2+} have a single band crossing E_F, which is usually described by the one-band Hubbard model.[7,8] By contrast, iron-based superconductors with Fe $3d^6$ electronic configuration have a multi-band and multi-orbital nature.[5] Moreover, cuprate shows a pseudogap above the transition temperature,[6] while Fe-SCs are usually bad metals in the normal state. To understand the importance of these similarities and differences in unconventional superconductivity, it is highly desired to explore new materials with HTSC.

Infinite-layer nickel oxides are considered to exhibit unconventional superconductivity despite their relatively low critical temperature.[9–13] Similar to the cuprates and Fe-SCs, $3d$ electrons of Ni dominate the electronic states near E_F. Electronic correlation also plays an important role in the electronic structure and superconductivity of Ni-based superconductors (Ni-SCs).[14] In particular, Ni^+ exhibits an effective electronic configuration of $3d^9$, the same as Cu^{2+} in cuprates,[15,16] making infinite-layer nickelates an attractive platform for exploring HTSC. Superconductivity at 15 K and 30 K has been observed in thin films of infinite-layer nickelates at ambient and high pressure respectively.[17,18] Superconductivity at 13 K is also ob-

†These authors contributed equally to this work.
*Corresponding authors. Email: qiyp@shanghaitech.edu.cn; hjguo@sslab.org.cn; yulin.chen@physics.ox.ac.uk; lxyang@tsinghua.edu.cn
© 2024 Chinese Physical Society and IOP Publishing Ltd

served in the quintuple-layer $Nd_6Ni_5O_{12}$, in which Ni exhibits an effective electronic configuration of $d^{8.8}$.[19] However, the synthesis of these nickelates is challenging and the superconductivity is realized only in thin films below the McMillan limit regardless of the application of pressure.

Recently, HTSC with T_c up to 80 K was discovered in $La_3Ni_2O_7$ bulk compound under pressure between 14.0 GPa and 43.5 GPa.[20–23] It belongs to the series of $La_{n+1}Ni_nO_{3n+1}$ Ruddlesden–Popper phase that can be viewed as the parent phase of the infinite-layer and quintuple-layer nickelates. Many theoretical understandings of the electronic structure and superconductivity of the system have been proposed.[24–35] It was proposed that the Ni ions with an average valence of +2.5 are pressurized to resemble the electronic configuration of Cu^{2+} in cuprates, which favors the superconductivity at high pressure.[20] Simultaneously, the crystal and electronic structures are strongly modulated by the pressure-induced Jahn–Teller distortion. The $3d_{x^2-y^2}$ and $3d_{z^2}$ orbitals strongly interact with O p orbitals, forming intra- and inter-layer σ bonds, respectively. The interaction between the occupied Ni $d_{x^2-y^2}$ and O p orbitals also induces the Zhang–Rice singlet in the superconducting state.[20,33] While it is extremely challenging to experimentally investigate the electronic structure at high pressure, the experiments at ambient pressure will nevertheless provide crucial information for its normal-state properties, including the Fermiology, the electronic correlation effect, density wave orders, and non-Fermi-liquid behaviors.[36–39] A previous measurement using angle-resolved photoemission spectroscopy (ARPES) revealed orbital dependent correlation effect in $La_3Ni_2O_7$ at ambient pressure[40] with more details awaiting further experimental exploration.

In this work, by combining ARPES and *ab initio* calculation, we systematically investigate the electronic structure of $La_3Ni_2O_7$ at ambient pressure. The band structure shows a multi-band and multi-orbital nature with Ni $3d_{x^2-y^2}$ and $3d_{z^2}$ orbitals dominating the electronic states near E_F.[24] After being renormalized by 2.7 and 5.0 for the $d_{x^2-y^2}$ and d_{z^2} bands respectively,[40] the calculated results are in nice agreement with the experiments, suggesting a strong electronic correlation in the system.[26–28,34,39] In particular, the $3d_{z^2}$ orbitals form a flat band just below E_F, which contributes significantly to the electronic density of states (DOS). With high pressure, our *ab initio* calculation suggests that the band width of the $La_3Ni_2O_7$ increases and the flat band locates right at E_F, which may favor the pressurized HTSC. Furthermore, we observe diminished quasiparticle peak and suppressed spectral weight as the $d_{x^2-y^2}$ band dispersing approaching E_F, which shows a pseudogap-like behavior with decreasing temperature and is reminiscent of the normal-state behaviors of cuprates and Fe-SCs.[8,41] Our findings will help construct a unified picture of unconventional HTSC in different families of materials.

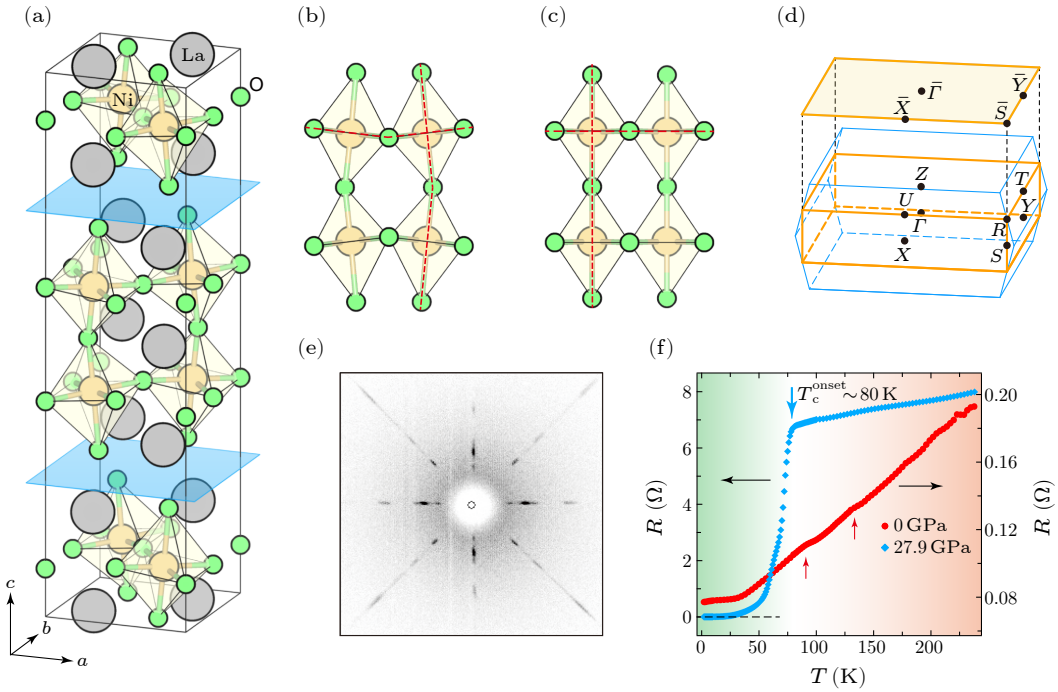

Fig. 1. Basic properties of $La_3Ni_2O_7$. (a) Schematic illustration of the crystal structure of $La_3Ni_2O_7$. The blue plane indicates the cleavage plane. [(b), (c)] The side view of the NiO_6 bilayer at ambient (b) and high (c) pressure. The red lines indicate the distortion and alignment of the octahedrons at ambient and high pressure. (d) Brillouin zone (BZ) of the conventional (orange lines) and primitive (blue lines) unit cells at ambient pressure. Surface projection and high symmetry points of the conventional BZ are also shown. (e) Laue pattern showing the orthorhombic structure of the crystal. (f) Resistance as a function of temperature at ambient and high-pressure. Superconducting transition under the pressure of 27.9 GPa at about 80 K is indicated by the blue arrow. The red arrows indicate the kink-like features in the resistance.

As schematically shown in Fig. 1(a), $La_3Ni_2O_7$ crystallizes into a layered orthorhombic structure in the space group *Amam* at ambient pressure with lattice constants $a = 5.393$ Å, $b = 5.449$ Å, and $c = 20.518$ Å.[20,42] In the conventional unit cell, corner-sharing NiO_6 octahedrons form Ni–O bilayers stacking along the c direction, which are separated by La–O layers. At ambient pressure, the NiO_6 octahedrons slightly distort with their vertical axis canting for about 6° away from the c axis [Fig. 1(b)].[20] The application of high pressure aligns the octahedrons along c and drives the system into the space group *Fmmm* [Fig. 1(c)]. The Ni–O planes also become flat at high pressure. Within each Ni–O bilayer, the corner-sharing of NiO_6 octahedrons through the apical oxygen atoms provides the structural basis for the interlayer σ bonds between Ni $3d_{z^2}$ and O p orbitals.[20] The crystals can be easily cleaved between the bilayers to expose the La–O termination as indicated by the blue planes in Fig. 1(a). The Brillouin zones (BZs) corresponding to the primitive and conventional unit cells are shown in Fig. 1(d) with high-symmetry points of the conventional BZ indicated.

Our sample shows clear Laue peaks in Fig. 1(e), confirming its orthorhombic structure. The metallic temperature dependence of the resistance suggests the proper element composition, particularly of the oxygen, since a slight deficiency of oxygen will drive the system into an insulating phase.[43] We note slight kink-like features in the resistance curve, which were previously associated to a possible charge-density-wave (CDW) transition.[22,44] At the pressure of 27.9 GPa, our samples show a superconducting transition with onset critical temperature of about 80 K [Fig. 1(f)], in good agreement with the previous measurements.[20,45]

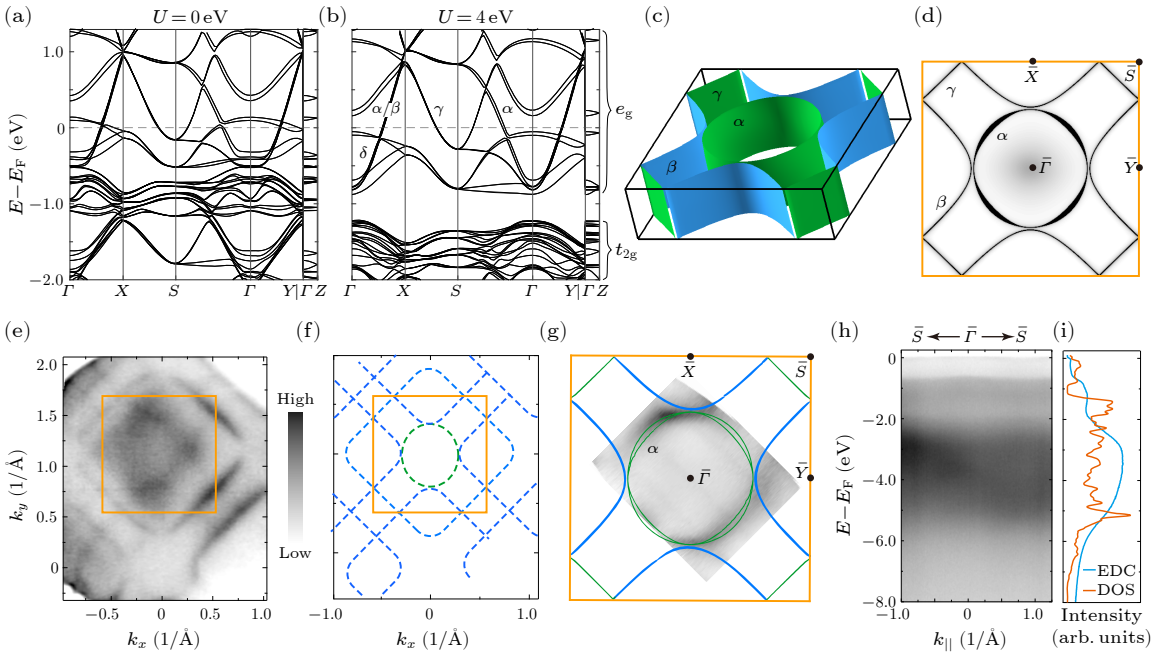

Fig. 2. Band structure of $La_3Ni_2O_7$. [(a), (b)] Calculated band structure at the ambient pressure with on-site Coulomb interaction on Ni atoms of $U = 0$ (a) and $U = 4$ eV (b). (c) Calculated three-dimensional (3D) Fermi surface (FS) shown in the conventional BZ. (d) Surface-projected FS calculation (surface-projected calculation of the band dispersions is shown in the Supplementary Information). (e) FS map measured by integrating ARPES intensity in an energy window of 40 meV around E_F. Please note that data were collected in the second BZ. (f) FS extracted from panel (e) according to ARPES intensity. The orange lines are the BZ of the conventional unit cell. (g) FS measured using a 7 eV laser at 40 K. ARPES intensity was integrated in an energy window of 40 meV around E_F. The calculated FS in the conventional BZ is overlaid for comparison. (h) Band dispersion measured in a large energy range along the $\bar{\Gamma}\bar{S}$ direction. (i) Comparison between the integrated energy distribution curve (EDC) and calculated density of states (DOS). Data in (e), (h), and (i) were collected using linear-horizontally (LH) polarized photons at 75 eV at 18 K.

Figures 2(a) and 2(b) show the *ab initio* calculation of the band structure at the ambient pressure with on-site Coulomb interaction on Ni atoms $U = 0$ eV and 4 eV, respectively. The on-site Coulomb interaction expels the t_{2g} bands towards higher binding energies, so that the e_g and t_{2g} bands do not hybridize for $U = 4$ eV. Simultaneously, the δ band with a flat band top submerges below E_F. Figure 2(c) shows the calculated three-dimensional (3D) Fermi surface (FS), which suggests a weak k_z dispersion, consistent with our experiments at different photon energies (see the Supplementary Information). There are three sets of FS sheets in the conventional BZ: a cylindrical electron pocket around the $\bar{\Gamma}$ point, a cylindrical hole pocket around the $\bar{X}/\bar{Y}$ point, and a flat FS sheet near the $\bar{S}$ point [Figs. 2(c) and 2(d)]. In the experiment, we observe a large rectangular pocket around the

$\bar{\Gamma}$ point [Fig. 2(e)], which originates from the band folding induced by the distortion [Figs. 1(a) and 1(c)] of the NiO_6 octahedrons at the ambient pressure (see the Supplementary Information). In the conventional BZ (orange lines) [Fig. 2(f)], we resolve a hole pocket around the $\bar{X}/\bar{Y}$ point and a small square-like pocket around the $\bar{S}$ point, agreeing nicely with the calculation. The parallel FS provides an ideal condition for FS nesting (see the Supplementary Information), which may drive an instability towards long-range ordering states,[22] as suggested by the calculation of the spin susceptibility.[46,47] However, the existence of the density-wave ordering and its origin require further experimental and theoretical investigations. The electron pocket around $\bar{\Gamma}$ is better visualized using laser-ARPES, consistent with the previous report.[40] Based on the experimental FS in Figs. 2(e) and 2(g), the carrier density is estimated to be about $0.249e^-$ per unit cell, in nice agreement with the theoretical predictions.[20] Figure 2(h) shows the band structure measured in a large energy range. The most prominent spectral features locate between −5.0 and −1.5 eV, with relatively weak intensity near E_F. The comparison between the integrated energy-distribution curve (EDC) and calculated DOS shows an overall consistence [Fig. 2(i)].

Figure 3 investigates the fine electronic structure near E_F. The 3D volume plot in Fig. 3(a) shows the overall band dispersion along different momentum directions. We observe a hole band δ with a flat band top and an electron band α/β around the $\bar{\Gamma}'$ point (the center of the second Brillouin zone) [Figs. 3(b) and 3(c)]. The flat band is very close to E_F, compared to that at about 50 meV below E_F in the previous ARPES measurements.[40] This difference might be due to the oxygen vacancies in the samples. The electron band α/β was also observed in the second BZ and at other photon energies (see the Supplementary Information). Near the $\bar{S}$ point, we observe an electron band γ dispersing to about 100 meV below E_F [Figs. 3(b) and 3(d)]. Data collected using 75 eV and 86 eV are in general similar to each other, consistent with the layered crystal structure [Figs. 3(c) and 3(e)]. It is noteworthy that the experimental band structure of $La_3Ni_2O_7$ is very similar to that of $La_4Ni_3O_{10}$,[48] which also shows superconductivity at high pressure.[49–51]

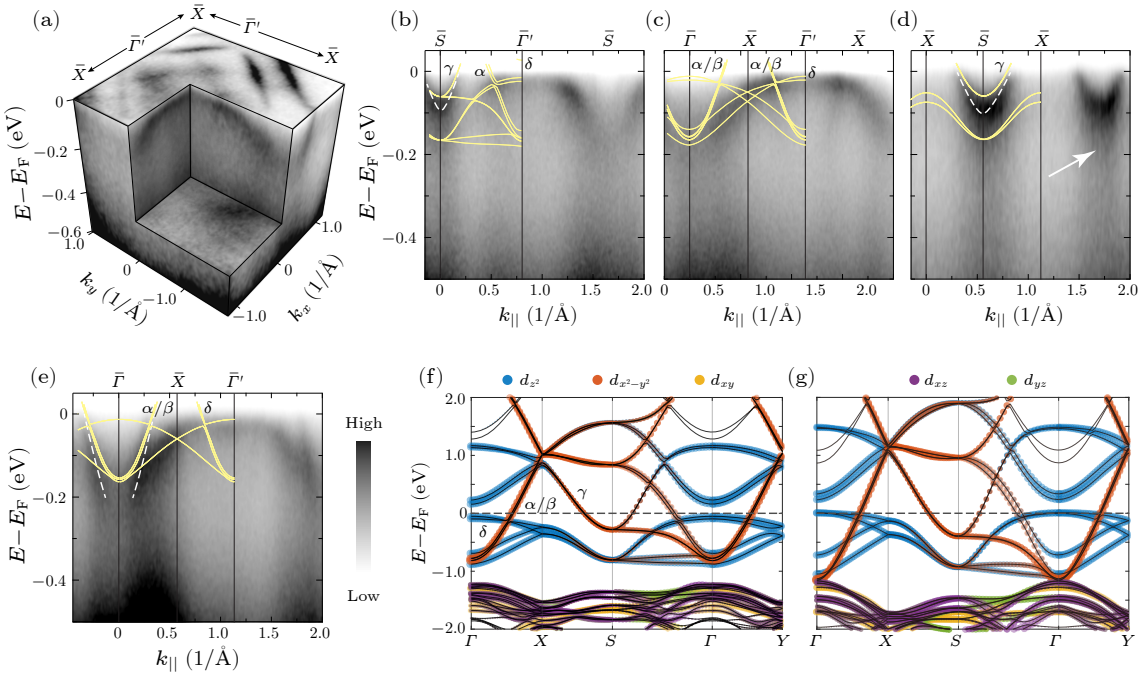

Fig. 3. Fine band dispersions along high-symmetry directions. (a) Three-dimensional plot of the electronic structure of $La_3Ni_2O_7$. [(b), (c), (d)] Band dispersions along the $\bar{\Gamma}'\bar{S}$ (b), $\bar{\Gamma}\bar{X}$ (c), and $\bar{X}\bar{S}$ (d) directions. Data in (a)–(d) were collected using LH polarized photons at 75 eV at 18 K. (e) Band dispersions along $\bar{\Gamma}\bar{X}$ measured using LH polarized photons at 86 eV at 18 K. The yellow curves are calculated band structure for comparison, which are renormalized by a factor of 5. The white dashed lines are of guide to the eyes for the experimental band dispersions to indicate the orbital-selective renormalization factors. [(f), (g)] Orbital-projected band structures at ambient pressure (f) and high pressure (g) with on-site Coulomb interaction $U = 4$ eV. The size of the circles represents the weight of the projected orbitals.

The calculated band structure with $U = 4$ eV is renormalized by a factor of about 5 and overlaid on the ARPES spectra in Figs. 3(b) and 3(e). The calculation nicely reproduces the experimental band structure, suggesting a strong electronic correlation in the system.[28,39] Consistently, we notice a waterfall-like structure at high energies, which has been widely observed in various correlated superconductors [white arrow in Fig. 3(d)].[52,53] It is noteworthy that the α/β and γ bands, with the estimated renormalization factor of about 2.7, are less-

correlated than the flat δ band, in agreement with the orbital-dependent electronic correlation effect in the previous report,[40,46] as indicated by the white dashed lines in Figs. 3(b), 3(d), and 3(e). By comparing with the orbital-projected calculation in Fig. 3(f) (see the Supplementary Information), we identify that the highly dispersive α/β band and the flat δ band are contributed by Ni $3d_{x^2-y^2}$ and $3d_{z^2}$ orbitals, respectively.[25,27,40] The electronic correlation and its orbital-dependence agree with previous ARPES experiment, while the latter reported a further enhancement of the correlation effect of the $3d_{z^2}$ band along the $\bar{\Gamma}\bar{S}$ direction.[40]

The nice agreement between the experiments and calculations confirms the validity of our *ab initio* calculations in the investigation of the electronic structure of $La_3Ni_2O_7$. We further calculated the band structure at high pressure that flattens the Ni–O layer and aligns NiO_6 octahedrons along c. As shown in Fig. 3(g), the bandwidth increases by about 25% and the δ band (the flat band in the experiment) moves closer to E_F. Moreover, a van Hove singularity (saddle point) at the $\bar{X}$ point also moves closer to E_F. Along $\bar{\Gamma}\bar{S}$ the $d_{x^2-y^2}$ and d_{z^2} orbitals show an enhanced mixture at high pressure. These changes of the band structure at high pressure will enhance the electronic DOS near E_F, which favors the superconducting transition.

Figure 4 investigates the temperature evolution of the electronic structure. With increasing temperature, the flat band stays put at temperatures up to about 120 K [Fig. 4(a)], as can be seen from the EDCs at $\bar{\Gamma}'$ [Fig. 4(b)]. We notice that the spectral weight of the α/β band gradually reduces as approaching E_F without a clear quasiparticle peak near E_F, which is also noticeable in Ref. [40] and is beyond the expectation of the typical Fermi-liquid picture. This behavior is better visualized in the laser-based ARPES measurements with improved energy and momentum resolutions as shown in Fig. 4(c). In a large temperature range from 19 K to 120 K, the spectral weight of the α band remains strongly suppressed near E_F. The degree of the suppression reduces with increasing temperature, which is evident by the gradual shift of the leading edge of the EDCs at k_F [Fig. 4(b)] towards high energies. The leading edge is below E_F even at 120 K, which may be related to the multiple kink-like features in the resistance that are related to the density-wave states[36–39,54] [Fig. 1(f)]. Figure 4(d) plots the leading-edge position as a function of temperature. It is clear that the leading-edge shift towards high-energies starts at about 100 K and reaches its maximum of about 9 meV at 19 K, showing a Bardeen–Cooper–Schrieffer (BCS)-like evolution.

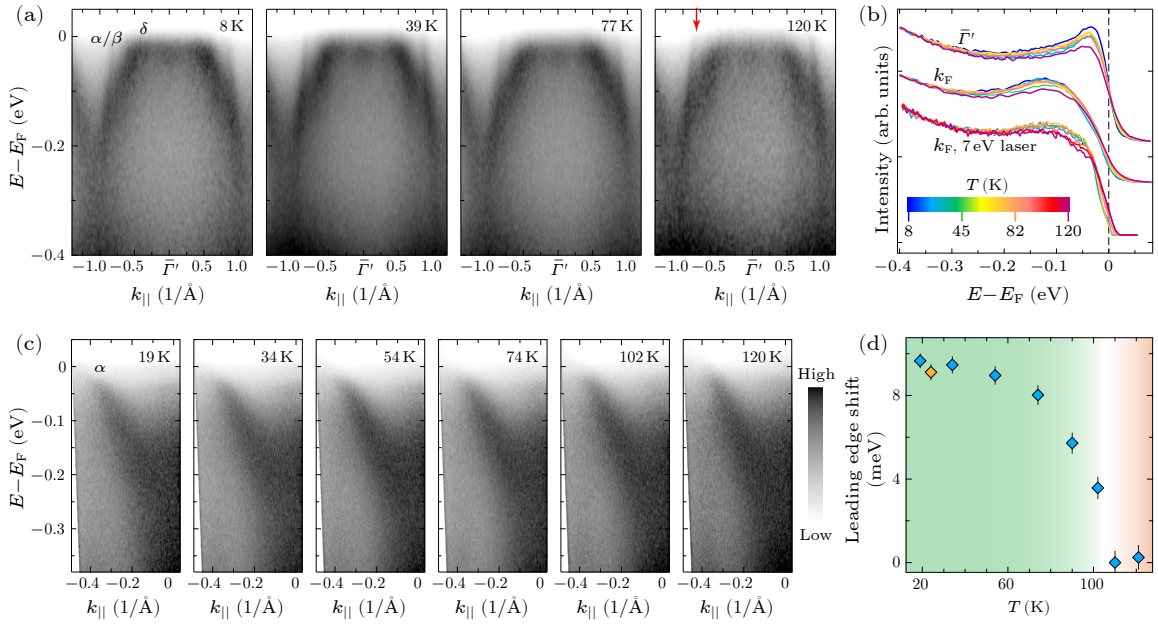

Fig. 4. Temperature-dependent ARPES measurements of $La_3Ni_2O_7$. (a) Band dispersions along $\bar{\Gamma}\bar{X}$ measured at selected temperatures. Data were collected using photons at 86 eV with LH polarization. (b) EDCs integrated around the $\bar{\Gamma}'$ point [data in (a)], $k_F = -0.8$ Å^{-1} [the red arrow in (a)], and $k_F = 0.39$ Å^{-1} [data in (c)] at selected temperatures. The EDCs are normalized by ARPES intensity in an energy window of 0.1 eV near −0.4 eV. (c) Band dispersions along $\bar{\Gamma}\bar{S}$ measured at selected temperatures. Data were collected using liner-vertically (LV) polarized laser at 7 eV. EDCs integrated near k_F (red arrow) at selected temperatures are shown in panel (b). (d) EDC leading edge shift at $k_F = 0.39$ Å^{-1} [data in (c)] with respect to the data at 110 K as a function of temperature. Aging effect has been excluded by temperature cycling measurement [the orange data point at 18 K in (d)].

The temperature dependence of the $d_{x^2-y^2}$ band is reminiscent of the pseudogap in cuprate superconductors,[6,8] However, one should notice that the observed pseudogap-like behavior is unnecessarily related to the HTSC under pressure. It is also noteworthy that recent theoretical calculations likewise unravel a pseudogap

in the DOS near E_F,[55] in agreement with our experiments. We suggest that the observed pseudogap-like behavior of $La_3Ni_2O_7$ may be due to the strong electronic correlation, the formation of possible density wave, and/or the hybridization between the "localized" d_{z^2} orbital and "itinerant" $d_{x^2-y^2}$ orbitals, which proposes further experimental and theoretical studies. On the other hand, the lacking of a well-defined Fermi edge in a metallic system suggests a non-Fermi-liquid behavior. Consistent with our observation, a non-Fermi-liquid behavior has also been revealed by the optical study[39] and our ultrafast reflectivity measurements.[56] Moreover, a non-Fermi-liquid state has been theoretically predicted in the *Fmmm* phase of $La_3Ni_2O_7$ at high pressure, which is argued to be intimately correlated to the superconducting state.[26]

In conclusion, we have comprehensively studied the electronic structure of $La_3Ni_2O_7$ at ambient pressure. The nice agreement between experiment and calculation with on-site Coulomb interaction and band renormalization suggests an important role of electronic correlation in the system. The d_{z^2} band is flattened by the strong correlation, while the less-correlated $d_{x^2-y^2}$ band shows pseudogap-like behavior, which are reminiscent of the orbital-selective band renormalization in Fe-SCs and pseudogap in cuprates. At high pressure, the flat band is predicted to locate right at E_F and is believed to be crucial for the HTSC. Our systematic experiments provide an electronic basis for exploring the Ni-based unconventional HTSC.

Methods. In the sample growth, single crystals of $La_3Ni_2O_7$ were grown by the high-pressure optical floating zone technique.[44] Raw materials of La_2O_3 were dried at 900 ℃ overnight prior to the reaction to avoid moisture contamination. Subsequently, La_2O_3 and NiO powders were mixed in a stoichiometric ratio with 1% ∼ 2% excess of NiO and then ground thoroughly. The mixture was then pressed into pellets and sintered at 1100 ℃ for two days with several intermediate grindings. The reactant was pressed into seed and feed rods with a diameter of about 6 mm under hydrostatic pressure and then sintered at 1300 ℃ for two hours. The single-crystal growth was performed in a high-pressure optical floating zone furnace (HKZ-300) with an oxygen pressure of 15 bar. The growth rate was 2 mm/h and the feed and seed rods were rotated in opposite directions with speeds of 20 and 25 rpm, respectively.

In our high-pressure transport measurement, high-pressure *in situ* electrical transport property was performed in a physical property measurement system (PPMS-9T) as described elsewhere.[57–59] Nonmagnetic BeCu diamond anvil cell (DAC) with 200 μm culet was employed to perform the *in situ* high-pressure resistivity measurements. A cubic-BN/epoxy mixture covers BeCu gasket as an insulator layer. The van der Pauw four-probe electrodes were applied on the cleavage plane. The pressure was determined by the ruby fluorescence method.[60]

Synchrotron-based ARPES measurements were conducted at beamline 03U in Shanghai Synchrotron Radiation Facility (SSRF). The samples were cleaved *in situ* under ultra-high vacuum below 7×10^{-11} mbar. Data were collected with a Scienta DA30 electron analyzer. The total energy and angular resolutions were set to 20 meV and 0.2°, respectively.

Laser-based ARPES measurements were conducted at Tsinghua University. The 7-eV laser was generated by frequency doubling in a KBBF crystal and focused on the sample by an optical lens. Samples were cleaved *in situ* under ultra-high vacuum below 6×10^{-11} mbar. Data were collected with a Scienta DA30L electron analyzer. The total energy and angular resolutions were set to 3 meV and 0.2°, respectively.

First-principles band structure calculations were performed using the Vienna *ab initio* simulation package (VASP)[61] with a plane wave basis. The exchange-correlation energy was considered under Perdew–Burke–Ernzerhof-type generalized gradient approximation (GGA)[62] with spin-orbit coupling included. Hubbard $U = 4$ eV was applied to describe the localized 3*d* orbitals of Ni atoms. The cutoff energy for the plane-wave basis was set to 400 eV. A Γ-centered Monkhorst–Pack *k*-point mesh of $19 \times 19 \times 5$ was adopted in the self-consistent calculations. Based on the tight-binding type Hamiltonian constructed from maximally localized Wannier functions (MLWF) supplied by the Wannier90 code,[63] the surface-projected band structures were calculated with the WANNIERTOOLS package.[64]

Acknowledgments. This work was supported by the National Key R&D Program of China (Grant Nos. 2022YFA1403100 and 2022YFA1403200), the National Natural Science Foundation of China (Grant Nos. 12275148, 12004270, and 52272265), and Guangdong Basic and Applied Basic Research Foundation (Grant No. 2022B1515120020). L. X. Y. acknowledges the support from Tsinghua University Initiative Scientific Research Program.

References

[1] Keimer B, Kivelson S A, Norman M R, Uchida S, and Zaanen J 2015 *Nature* **518** 179
[2] Zhou X J, Lee W S, Imada M, Trivedi N, Phillips P, Kee H Y, Törmä P, and Eremets M 2021 *Nat. Rev. Phys.* **3** 462
[3] Si Q, Yu R, and Abrahams E 2016 *Nat. Rev. Mater.* **1** 16017
[4] Tsuei C C and Kirtley J R 2000 *Rev. Mod. Phys.* **72** 969
[5] Paglione J and Greene R L 2010 *Nat. Phys.* **6** 645
[6] Hashimoto M, Vishik I M, He R H, Devereaux T P, and Shen Z X 2014 *Nat. Phys.* **10** 483
[7] Dagotto E 1994 *Rev. Mod. Phys.* **66** 763
[8] Damascelli A, Hussain Z, and Shen Z X 2003 *Rev. Mod. Phys.* **75** 473
[9] Zhou X, Qin P, Feng Z, Yan H, Wang X, Chen H, Meng Z, and Liu Z 2022 *Mater. Today* **55** 170
[10] Li D, Lee K, Wang B Y, Osada M, Crossley S, Lee H R, Cui Y, Hikita Y, and Hwang H Y 2019 *Nature* **572** 624
[11] Pickett W E 2021 *Nat. Rev. Phys.* **3** 7
[12] Li D, Wang B Y, Lee K, Harvey S P, Osada M, Goodge B H, Kourkoutis L F, and Hwang H Y 2020 *Phys. Rev. Lett.* **125** 027001
[13] Osada M, Wang B Y, Goodge B H, Harvey S P, Lee K, Li D, Kourkoutis L F, and Hwang H Y 2021 *Adv. Mater.* **33** 2104083

[14] Kreisel A, Andersen B M, Rømer A T, Eremin I M, and Lechermann F 2022 *Phys. Rev. Lett.* **129** 077002
[15] Hepting M, Li D, Jia C J *et al.* 2020 *Nat. Mater.* **19** 381
[16] Sakakibara H, Usui H, Suzuki K, Kotani T, Aoki H, and Kuroki K 2020 *Phys. Rev. Lett.* **125** 077003
[17] Zeng S W, Li C J, Chow L E *et al.* 2022 *Sci. Adv.* **8** eabl9927
[18] Wang N N, Yang M W, Yang Z *et al.* 2022 *Nat. Commun.* **13** 4367
[19] Pan G A, Ferenc Segedin D, LaBollita H *et al.* 2022 *Nat. Mater.* **21** 160
[20] Sun H L, Huo M W, Hu X W *et al.* 2023 *Nature* **621** 493
[21] Hou J, Yang P T, Liu Z Y, Li J Y, Shan P F, Ma L, Wang G, Wang N N, Guo H Z, Sun J P, Uwatoko Y, Wang M, Zhang G M, Wang B S, and Cheng J G 2023 *Chin. Phys. Lett.* **40** 117302
[22] Zhang Y N, Su D J, Huang Y N, Shan Z Y, Sun H L, Huo M W, Ye K X, Zhang J W, Yang Z H, Xu Y K, Su Y, Li R, Smidman M, Wang M, Jiao L, and Yuan H Q 2024 *Nat. Phys.* (accepted)
[23] Zhang M X, Pei C Y, Wang Q, Zhao Y, Li C H, Cao W Z, Zhu S H, Wu J F, and Qi Y P 2024 *J. Mater. Sci. Technol.* **185** 147
[24] Luo Z H, Hu X W, Wang M, Wú W, and Yao D X 2023 *Phys. Rev. Lett.* **131** 126001
[25] Zhang Y, Lin L F, Moreo A, and Dagotto E 2023 *Phys. Rev. B* **108** L180510
[26] Lechermann F, Gondolf J, Bötzel S, and Eremin I M 2023 *Phys. Rev. B* **108** L201121
[27] Cao Y and Yang Y F 2024 *Phys. Rev. B* **109** L081105
[28] Liao Z, Chen L, Duan G, Wang Y, Liu C, Yu R, and Si Q 2023 *Phys. Rev. B* **108** 214522
[29] Shen Y, Qin M, and Zhang G M 2023 *Chin. Phys. Lett.* **40** 127401
[30] Gu Y H, Le C C, Yang Z S, Wu X X, and Hu J P 2023 arXiv:2306.07275 [cond-mat.supr-con]
[31] Yang Y f, Zhang G M, and Zhang F C 2023 arXiv:2308.01176 [cond-mat.supr-con]
[32] Tian Y H, Chen Y, Wang J M, He R Q, and Lu Z Y 2024 *Phys. Rev. B* **109** 165154
[33] Wu W, Luo Z H, Yao D X, and Wang M 2024*Sci. China Phys. Mech. Astron.* **67** 117402
[34] Christiansson V, Petocchi F, and Werner P 2023 *Phys. Rev. Lett.* **131** 206501
[35] Zhang J X, Zhang H K, You Y Z, and Weng Z Y 2023 arXiv:2309.05726 [cond-mat.supr-con]
[36] Chen X Y, Choi J, Jiang Z C, Mei J, Jiang K, Li J, Agrestini S, Garcia-Fernandez M, Huang X, Sun H L, Shen D W, Wang M, Hu J P, Lu Y, Zhou K J, and Feng D L 2023 arXiv:2401.12657 [cond-mat.supr-con]
[37] Dan Z, Zhou Y B, Huo M W, Wang Y, Nie L P, Wang M, Wu T, and Chen X H 2024 arXiv:2402.03952 [cond-mat.supr-con]
[38] Chen K W, Liu X Q, Jiao J C *et al.* 2024 *Phys. Rev. Lett.* **132** 256503
[39] Liu Z, Huo M W, Li J, Li Q, Liu Y C, Dai Y M, Zhou X X, Hao J H, Lu Y, Wang M, and Wen H H 2023 arXiv:2307.02950 [cond-mat.supr-con]
[40] Yang J, Sun H, Hu X, Xie Y, Miao T, Luo H, Chen H, Liang B, Zhu W, Qu G, Chen C Q, Huo M, Huang Y, Zhang S, Zhang F, Yang F, Wang Z, Peng Q, Mao H, Liu G, Xu Z, Qian T, Yao D X, Wang M, Zhao L, and Zhou X J 2024 *Nat. Commun.* **15** 4373
[41] Yi M, Lu D H, Yu R *et al.* 2013 *Phys. Rev. Lett.* **110** 067003
[42] Ling C D, Argyriou D N, Wu G, and Neumeier J J 2000 *J. Solid State Chem.* **152** 517
[43] Taniguchi S, Nishikawa T, Yasui Y, Kobayashi Y, Takeda J, Shamoto S i, and Sato M 1995 *J. Phys. Soc. Jpn.* **64** 1644
[44] Liu Z J, Sun H L, Huo M W *et al.* 2023 *Sci. China Phys. Mech.* **66** 217411
[45] The results about the superconductivity at high pressure will be presented elsewhere.
[46] Shilenko D A and Leonov I V 2023 *Phys. Rev. B* **108** 125105
[47] Wang Y X, Jiang K, Wang Z Q, Zhang F C, and Hu J P 2024 arXiv:2401.15097 [cond-mat.supr-con]
[48] Li H, Zhou X, Nummy T, Zhang J, Pardo V, Pickett W E, Mitchell J F, and Dessau D S 2017 *Nat. Commun.* **8** 704
[49] Zhang M X, Pei C Y, Du X, Hu W X, Cao Y T, Wang Q, Wu J F, Li Y D, Liu H Y, Wen C, Zhao Y, Li C H, Cao W Z, Zhu S H, Zhang Q, Yu N, Cheng P H, Zhang L L, Li Z W, Zhao J K, Chen Y L, Guo H J, Wu C J, Yang F, Yan S C, Yang L X, and Qi Y P 2023 arXiv:2311.07423 [cond-mat.supr-con]
[50] Zhu Y, Peng D, Zhang E, Pan B, Chen X, Chen L, Ren H, Liu F, Hao Y, Li N, Xing Z, Lan F, Han J, Wang J, Jia D, Wo H, Gu Y, Gu Y, Ji L, Wang W, Gou H, Shen Y, Ying T, Chen X, Yang W, Cao H, Zheng C, Zeng Q, Guo J G, and Zhao J 2024 *Nature* **631** 531
[51] Li Q, Zhang Y J, Xiang Z N, Zhang Y, Zhu X, and Wen H H 2024 *Chin. Phys. Lett.* **41** 017401
[52] Zhou J S, Xu R Z, Yu X Q *et al.* 2023 *Phys. Rev. Lett.* **130** 216004
[53] Xie B P, Yang K, Shen D W *et al.* 2007 *Phys. Rev. Lett.* **98** 147001
[54] Khasanov R, Hicken T J, Gawryluk D J, Sorel L P, Bötzel S, Lechermann F, Eremin I M, Luetkens H, and Guguchia Z 2024 arXiv:2402.10485 [cond-mat.supr-con]
[55] Lechermann F, Bötzel S, and Eremin I M 2024 *Phys. Rev. Mater.* **8** 074802
[56] Li Y D, Cao Y T, Liu L Y, Peng P, Lin H, Pei C Y, Zhang M X, Wu H, Du X, Zhao W X, Zhai K Y, Zhao J K, Lin M L, Tan P H, Qi Y P, Li G, Guo H J, Yang L Y, and Yang L X 2024 arXiv:2403.05012 [cond-mat.supr-con]
[57] Pei C Y, Zhang J F, Wang Q *et al.* 2023 *Natl. Sci. Rev.* **10** nwad034
[58] Pei C Y, Ying T P, Zhang Q H *et al.* 2022 *J. Am. Chem. Soc.* **144** 6208
[59] Wang Q, Kong P F, Shi W J *et al.* 2021 *Adv. Mater.* **33** 2102813
[60] Mao H K, Xu J, and Bell P M 1986 *J. Geophys. Res.* **91** 4673
[61] Kresse G and Furthmüller J 1996 *Phys. Rev. B* **54** 11169
[62] Perdew J P, Burke K, and Ernzerhof M 1996 *Phys. Rev. Lett.* **77** 3865
[63] Mostofi A A, Yates J R, Lee Y S, Souza I, Vanderbilt D, Marzari N 2008 *Comput. Phys. Commun.* **178** 685
[64] Wu Q, Zhang S, Song H F, Troyer M, and Soluyanov A A 2018 *Comput. Phys. Commun.* **224** 405